Human *RAP2A* Homolog of the *Drosophila* Asymmetric Cell Division Regulator *Rap2l* Targets the Stemness of Glioblastoma Stem Cells

Maribel Franco[1], Ricardo Gargini[2], Víctor M. Barberá[3, 4], Daniel Becerra[1], Miguel Saceda[4] and Ana Carmena[1*]

[1]Instituto de Neurociencias, Consejo Superior de Investigaciones Científicas/Universidad Miguel Hernández de Elche, Sant Joan d'Alacant 03550, Alicante, Spain

[2]Instituto de Investigación Biomédicas I+12 and Pathology and Neurooncology Unit, Hospital Universitario 12 de Octubre, Madrid 28041, Spain

[3]Unidad de Genética Molecular, Hospital General Universitario de Elche, Camí del'Almazara 11, Elche, 03203, Alicante, Spain

[4]Unidad de Investigación, Fundación para el Fomento de la Investigación Sanitaria y Biomédica de la Comunidad Valenciana (FISABIO), Hospital General Universitario de Elche, Camí del'Almazara 11, Elche, 03203, Alicante, Spain

Running title: Human RAP2A Targets the Stemness of GSCs

***Corresponding author:** acarmena@umh.es; Instituto de Neurociencias, Consejo Superior de Investigaciones Científicas/Universidad Miguel Hernández de Elche, 03550-Sant Joan d'Alacant, Alicante, Spain

Abstract

Asymmetric cell division (ACD) is a fundamental process to balance cell proliferation and differentiation during development and in the adult. Cancer stem cells (CSCs), a very small but highly malignant population within many human tumors, are able to provide differentiated progeny by ACD that contribute to the intratumoral heterogeneity, as well as to proliferate without control by symmetric, self-renewing divisions. Thus, ACD dysregulation in CSCs could trigger cancer progression. Here we consistently find low expression levels of *RAP2A*, the human homolog of the *Drosophila* ACD regulator *Rap2l*, in glioblastoma (GBM) patient samples, and observe that scarce levels of *RAP2A* are associated with poor clinical prognosis in GBM. Additionally, we show that restitution of RAP2A in GBM neurosphere cultures increases the ACD of glioblastoma stem cells (GSCs), decreasing their proliferation and expression of stem cell markers. Our results support that ACD failures in GSCs increases their spread, and that ACD amendment could contribute to reduce the expansion of GBM.

49 **Introduction**

50 Asymmetric cell division (ACD) is a universal mechanism for generating cellular
51 diversity during development as well as for regulating tissue homeostasis in the adult
52 (1). Stem and progenitor cells undergo ACD to simultaneously give rise to a self-
53 renewing stem/progenitor cell and to a daughter cell that is committed to enter a
54 differentiation program. Remarkably, over the past years it has become apparent that
55 undermining this critical process can lead to tumor-like overgrowth (2). This link
56 between failures in the process of ACD and tumorigenesis was first established using
57 the *Drosophila* neural stem cells, called neuroblasts (NBs), as a model system (3). In
58 this work, authors showed how *Drosophila* larval mutant brains for ACD regulatory
59 genes were able to induce the formation of massive tumoral masses after weeks of
60 being transplanted into the abdomen of wild-type fly hosts. Intriguingly, some genes
61 firstly identified in *Drosophila* as tumor suppressor genes, such as *discs large 1* (*dlg1*),
62 *lethal (2) giant larvae* (*l(2)gl*) and *brain tumor* (*brat*) (4), were later uncovered as ACD
63 regulators (5-11), further supporting the connection between compromised ACD and
64 tumorigenesis.

65 Tumor initiating cells or cancer stem cells (CSCs) were originally identified in
66 acute myeloid leukemia (AML) (12,13) but, to date, several studies have also revealed
67 the existence of CSCs in multiple solid tumors (14). These CSCs represent a very small
68 but highly malignant population within the tumor, able to proliferate without control
69 by symmetrical, self-renewal divisions, as well as to provide differentiated progeny by
70 ACD that contribute to the heterogeneity of the tumor. These properties, along with
71 their quiescent state, increase in metabolic activity and high capacity of DNA repair,
72 make CSCs extremely resistant to radio- and chemotherapy and responsible for

73 malignant relapse (14-18). Thus, understanding the unique nature of these cells and
74 their landmarks is crucial to target CSCs and hence to completely destroy the tumor.
75 An intriguing possibility is that an imbalance in the mode of CSC divisions, favoring
76 symmetric renewal divisions in detriment of asymmetric divisions, might contribute to
77 the transition from a chronic (low grade) to an acute (high grade) phase in the cancer
78 progression (19,20).

79 Glioblastoma (GBM), the most aggressive and lethal brain tumor with very poor
80 prognosis, is among the solid tumors in which the presence of CSCs, called glioma or
81 glioblastoma stem cells (GSCs), has been proven. As other CSCs, GSCs are responsible
82 for the formation, maintenance, resistance to conventional therapy and consequent
83 relapse of GBM (21-25). Several GSC biomarkers, such as CD133 and Nestin, and
84 signaling pathways, such as Notch and Hedgehog, have been identified to help isolate
85 and target these crucial cells (14,26,27). Despite of that, there are still many unknowns
86 regarding the nature, properties and origin of CSCs in general and of GSCs in particular.

87 Here, we analyze the consequences of compromising ACD in the GSCs within
88 GBM neurosphere cell cultures. Specifically, we show that *RAP2A*, the human homolog
89 of *Rap2l*, which encodes a *Drosophila* small GTPase and novel ACD regulator, displays
90 low expression levels in GBM, and that restitution of RAP2A in GBM neurosphere
91 cultures increases the ACD and decreases the expression of stem cell markers in the
92 GSCs. Our results support that failures in ACD increase GSC proliferation promoting
93 their spreading and that ACD amendment might contribute to reduce the expansion of
94 GBM.

95

96

97 **Results**

98 **RAP2A is highly downregulated in GBM patients**

99 As a first approach to analyze whether ACD might be impaired in GBM, we analyzed
100 the expression levels of human homologs of 21 *Drosophila* ACD regulators in a GBM
101 microarray (28) (**Fig. 1A**). We also investigated which of those genes were more similar
102 in expression pattern to the others by performing a Gene Distance Matrix (**Fig. 1B**).
103 The human genes *TRIM2* and *RAP2A* showed the lowest levels in the GBM patient
104 samples analyzed. *TRIM2* belongs to the same family that *TRIM3* and *TRIM32*, all of
105 them related to the *Drosophila* ACD regulator gene *brat*. *TRIM3,* the closest homolog
106 of *brat*, has been previously found to be expressed at low levels in GBM (29). Hence,
107 we concentrated on *RAP2A*, the second human gene consistently found at very low
108 levels in all the patient samples (**Fig. 1A and Fig. S1**). *RAP2A* is also known to have a
109 tumor suppressor role in the context of glioma migration and invasion (30,31). First, to
110 further support the microarray data expression levels in a bigger sample size, we
111 performed *in silico* analyses taking advantage of established datasets of Glioblastoma
112 IDH wild-type, such as "The Cancer Genome Atlas" (TCGA) and "Gravendeel" cohorts.
113 We confirmed that low *RAP2A* expression levels in human GBM are associated with a
114 poor prognosis (**Fig. 1C**). In a multivariate analysis in the TCGA cohort, when we
115 included the variables RAP2A expression, patient age and standard
116 chemo/radiotherapy treatment in the model, it was observed that RAP2A levels and
117 patient age have a significant implication in patient survival as an independent
118 variable. In fact, specific values were significant in predicting overall survival (OS). For
119 example, "RAP2A expression" with a hazard ratio (HR) of 0.866 (95% CI 0.760-0.986)
120 and a *p*-value of 0.03, and "patient age" with a hazard ratio (HR) of 1.030 (95% CI

121 1.022-1.037) and a *p*-value of <0.001. Conversely, standard chemo/radiotherapy
122 treatment did not remain as an independent variable, with a hazard ratio (HR) of 0.820
123 and a *p*-value of 0.053. We also analyzed RAP2A levels in the different GBM subtypes
124 (proneural, mesenchymal and classical) in the TCGA cohort and their prognostic
125 relevance. The proneural subtype that displayed RAP2A levels significantly higher than
126 the others was the subtype that also showed better prognosis (**Fig. S2**). Hence, we
127 focused on the human gene *RAP2A* to analyze its potential role in ACD and its
128 relevance in GBM.
129
130 ***Drosophila RAP2A* homolog *Rap2l* regulates ACD**
131 We previously showed that the *Drosophila* gene *Rap1* regulates the ACD process (32).
132 The closest human homolog of *Drosophila Rap1* is *RAP1A*, while human *RAP2A* is more
133 similar to *Drosophila Rap2l,* which has not been previously analyzed in the context of
134 ACD. Hence, we first wanted to investigate whether *Rap2l* was, like *Rap1*, implicated in
135 ACD regulation. With that aim, we started analyzing the ACD of neural stem cells
136 (neuroblasts, NBs) and intermediate neural progenitors (INPs) within *Drosophila* larval
137 brain type II NB lineages (NBII) (**Fig. 2A**) (8,33,34). In NBII lineages, there is one NB that
138 expresses the transcription factor Deadpan (Dpn) and several INPs, which express both
139 Dpn and the transcription factor Asense (Ase) (**Fig. 2A**). We first observed the presence
140 of ectopic NBs (eNBs; Dpn^+ Ase^-) after downregulating *Rap2l* in NBII lineages in 4 out of
141 5 mutant brains analyzed (n = 34 NB lineages), while in control lineages only one NB
142 was usually found (**Fig. 2B**). To further determine the specificity and penetrance of the
143 phenotype, we repeated this experiment analyzing this and two additional *Rap2l* RNAi
144 lines, substantially increasing the number of the samples (both the number of NB

145 lineages and the number of brains analyzed) (**Fig. S3**). All the different lines showed a
146 highly significant number of ectopic NBs (**** $p < 0.001$; n> 120 NB lineages analyzed)
147 in all or almost all of the different brains analyzed (n>14) (see **Fig. S3** for details). This
148 result suggested that the process of ACD was impaired within those *Rap2l* mutant NBII
149 lineages. To more directly support that, we analyzed the localization of key ACD
150 regulators in metaphase NBs and INPs of NBII lineages, such as the apical proteins
151 aPKC and Canoe (Cno), and the cell-fate determinant Numb (35-37). In control
152 metaphase NBs and INPs, those ACD regulators form crescents at the apical (aPKC and
153 Cno) or basal (Numb) poles of the dividing cell (**Fig. 2C**). The apical localization of aPKC
154 was not significantly altered after downregulating *Rap2l* in NBII lineages; however, the
155 localization of Cno and Numb did fail in most of the *Rap2l* mutant brains analyzed (in 5
156 out of 6 in the case of Cno, and in 3 out of 4 in the case of Numb) (**Fig. 2C**). All these
157 results strongly suggested that Rap2l, as Rap1, was an ACD regulator. Hence, we came
158 back to the human homolog of *Drosophila Rap2l*, *RAP2A*, to determine its potential
159 relevance in the context of the ACD of GSCs.
160

161 **RAP2A expression in GBM neurosphere cultures reduces the stem cell population**

162 After confirming by *in silico* analyses that low *RAP2A* expression levels in GBM patients
163 were associated to a poor prognosis, we decided to use established GBM cell lines to
164 investigate in neurosphere cell cultures whether the downregulation of *RAP2A* was
165 affecting the properties of GSCs. We tested six different GBM cell lines finding similar
166 mRNA levels of *RAP2A* in all of them, and significantly lower levels than in control
167 Astros (**Fig. 3A**). We focused on the GBM cell line called GB5, which grew well in
168 neurosphere cell culture conditions, for further analyses. Given that stem cell markers,

169 such as CD133, SOX2 and NESTIN are landmarks of GSCs, we started analyzing their
170 expression after restoring RAP2A in the neurosphere culture (**Fig. 3B**).
171 Immunofluorescences of each of those markers revealed a significant reduction in the
172 protein intensity in the RAP2A-expressing neurospheres (GB5-RAP2A) compared to the
173 control neurospheres (GB5) (**Fig. 3C**). Likewise, RT-PCRs and Westerns blots also
174 showed a significant decrease in the mRNA and protein expression levels, respectively,
175 of those stem cell markers (**Fig. 4**). Hence, RAP2A seems to be contributing to decrease
176 the stem cell population within GBM neurosphere cultures.
177
178 **RAP2A expression in GBM neurosphere cultures decreases cell proliferation and**
179 **sphere size**
180 Next, we wondered whether the reduction in the stem cell population after expressing
181 *RAP2A* in neurosphere cultures was reflected in the level of cell proliferation and,
182 consequently, in the size of the neurospheres. To investigate this, we first analyzed the
183 expression of the proliferation marker and key tool in cancer diagnostics Ki-67, highly
184 expressed in cycling cells but absent in quiescent (G0) cells (38,39). We detected a
185 significant decrease in the number of proliferating cells per neurosphere in those
186 cultures expressing *RAP2A* (**Fig. 5A**). Moreover, the average area size of these GB5-
187 RAP2A neurospheres was also significantly reduced compared to control GB5
188 neurospheres (**Fig. 5B**). Thus, RAP2A promotes a decrease in cell proliferation.
189
190 **RAP2A expression in GBM neurosphere cultures fosters ACD in GSCs**
191 Given the reduction in cell proliferation and in the stem cell population after adding
192 RAP2A to the control GB5 neurosphere cultures, we wanted to investigate whether

193 RAP2A was favoring an asymmetric mode of cell division in these cells. Thus, we
194 decided to follow over time the GB5-RAP2A and the control GB5 neurospheres,
195 analyzing the number of cells per neurosphere. We reasoned that an even number of
196 cells per neurosphere would be indicative of symmetric cell divisions, while an odd
197 number of cells would point to an asymmetric mode of cell division (see also Material
198 and methods for details). We observed a significant increase of neurospheres with an
199 odd number of cells in the GB5-RAP2A neurospheres (n= 124 neurospheres analyzed)
200 compared to control GB5 neurospheres (n=153 neurospheres) (**Fig. 6A**). This result was
201 very suggestive of an increase in the number of ACDs in GB5-RAP2A neurosphere cells.
202 To further support this result, we decided to analyze the distribution of the cell fate
203 determinant NUMB, a key conserved ACD regulator whose asymmetric distribution in
204 the mother and progeny ultimately promotes the repression of stem cell self-renewal
205 in the daughter cell in which is segregated (40-44). We observed a significant increase
206 in the number of GB5-RAP2A dividing cells that showed an asymmetric localization of
207 NUMB in the progeny, compared to control GB5 dividing cells (**Fig. 6B**). Thus, all these
208 results strongly supported a function of RAP2A promoting ACD in the GSCs.
209

210 **Discussion**

211 ACD is an evolutionary conserved mechanism used by stem and progenitor cells to
212 generate cell diversity during development and to regulate tissue homeostasis in the
213 adult. CSCs, present in many human tumors, can divide asymmetrically to generate
214 intratumoral heterogeneity or symmetrically to expand the tumor by self-renewal.
215 Over the past 15 years, it has been suggested that dysregulation of the balance
216 between symmetric and asymmetric cell divisions in CSCs, favoring symmetric

217 divisions, can trigger tumor progression in different types of cancer (19,20,45)
218 including mammary tumors (43,46), glioblastoma (29), oligodendrogliomas (47,48),
219 colorectal cancer (49,50) and hepatocellular carcinoma (50). Thus, it is of great
220 relevance to get a deeper insight into the network of regulators that control ACD, as
221 well as the mechanisms by which they operate in this key process.

222 *Drosophila* neural stem cells or NBs have been used as a paradigm for many
223 decades to study ACD (51). NBs divide asymmetrically to give rise to another self-
224 renewing NB and a daughter cell that will start a differentiation process. Over all these
225 years, a complex network of ACD regulators that tightly modulate this process has
226 been characterized. For example, the so-called cell-fate determinants, including the
227 Notch inhibitor Numb, accumulate asymmetrically at the basal pole of mitotic NBs and
228 are exclusively segregated to one daughter cell, promoting in this cell a differentiation
229 process. The asymmetric distribution of cell-fate determinants in the NB is, in turn,
230 regulated by an intricate group of proteins asymmetrically located at the apical pole of
231 mitotic NBs, generically known as the "apical complex". This apical complex includes
232 kinases (i.e. aPKC), small GTPases (i.e. Cdc42, Rap1) and Par proteins (i.e. Par-6, Par3),
233 among others (51).

234 Given the potential relevance of ACD in CSCs, we decided to take advantage of
235 all the knowledge accumulated in *Drosophila* about the network of modulators that
236 control asymmetric NB division. As a first approach, we aimed to analyze whether the
237 levels of human homologs of known *Drosophila* ACD regulators were altered in human
238 tumors. Specifically, we centered on human GBM, as the presence of CSCs (GSCs) have
239 been shown in this tumor. The microarray we interrogated with GBM patient samples
240 had some limitations. For example, not all the human genes homologs of the

241 *Drosophila* ACD regulators were present (i.e. the human homologs of the determinant
242 Numb). Likewise, we only tested seven different GBM patient samples. Nevertheless,
243 the output from this analysis was enough to determine that most of the human genes
244 tested in the array presented altered levels of expression. We selected for further
245 analyses *RAP2A*, one of the human genes that showed the lowest levels of expression,
246 compared to the control samples. However, it would be interesting to analyze in the
247 future the potential consequences that altered levels of expression of the other human
248 homologs in the array can have in the behavior of the GSCs. In silico analyses, taking
249 advantage of the existence of established datasets, such as the TCGA, can help to more
250 robustly assess, in a bigger sample size, the relevance of those human genes
251 expression levels in GBM progression, as we observed for the gene *RAP2A*.

252 We have previously shown that *Drosophil*a Rap1 acts as a novel NB ACD
253 regulator in a complex with other small GTPases and the apical regulators Canoe (Cno),
254 aPKC and Par-6 (32). Here we have shown that *Drosophila* Rap2l also regulates NB ACD
255 by ensuring the correct localization of the ACD modulators Cno and Numb. We also
256 have demonstrated that RAP2A, the human homolog of *Drosophila* Rap2l, behaves as
257 an ACD regulator in GBM neurosphere cultures, and its restitution to these GBM
258 cultures, in which is present at low levels, targets the stemness of GSCs increasing the
259 number of ACDs. It would be of great interest in the future to determine the specific
260 mechanism by which Rap2l/RAP2A is regulating this process. One possibility is that, as
261 it occurs in the case of the *Drosophila* ACD regulator Rap1, Rap2l/RAP2A is physically
262 interacting or in a complex with other relevant ACD modulators. Thus, this study
263 supports the relevance of ACD in CSCs of human tumors to refrain the expansion of the
264 tumor. Other studies, however, claim that ACD should be targeted in human tumors as

265 it promotes the intratumoral heterogeneity that hampers the complete tumor loss
266 after chemotherapy (52-54). More investigations should be carried out with other
267 human genes homologs of ACD regulators to further confirm the results of this study.
268 Likewise, analyses in vivo (i.e. in mouse xenografts) would be also required to reinforce
269 our conclusions. This would be very relevant in order to consider ACD restitution in
270 CSCs of human tumors, what has been called "differentiation therapy" (55), as a
271 potential alternative therapeutic treatment.
272
273
274

275 **Materials and Methods**

276 ***Drosophila* husbandry, strains and genetics**

277 The following fly stocks were used: *wor-Gal4 ase-Gal80 (56)*; *UAS-CD8::GFP*
278 (Bloomington *Drosophila* Stock Center -BDSC- #5137); *UAS-CD2* (BDSC #1373); *UAS-*
279 *Rap2l*^{KKRNAi} (Vienna *Drosophila* Resource Center -VDRC- #107745); *UAS-Rap2l*^{GDRNAi}
280 (VDRC #45228)*; UAS-Rap2l*^{RNAi} (BDSC #51840); *cno::GFP (57)*. All the fly stocks were
281 raised and kept in 18°C or 25°C incubators. Experimental temperatures for the assays
282 were maintained using 25°C or 29°C incubators. The *Gal-4* x *UAS*-crosses were carried
283 out at 29°C (the first 2 days they were kept at 25°C, and then transferred to a new
284 tube and left at 29°C) until third instar larvae developed.

285

286 ***Drosophila* histology, immunofluorescence and microscopy**

287 Larval brains were dissected out in PBS and fixed with 4% PFA in PBT (PBS and Triton X-
288 100 0.1%) for 20 min at room temperature with gentle rocking. Fixed brains were
289 washed 3 times for 15 min with PBT (PBS and Triton X-100 0.3%) and then incubated in
290 PBT-BSA for at least 1h before incubation with the corresponding primary
291 antibody/antibodies. The following primary antibodies were used in this study: guinea
292 pig anti-Dpn (1:2,000) (57), rabbit anti-Ase (1:100) (57), rabbit anti PKCζ (1:100; Santa
293 Cruz Biotechnology, sc-216), goat anti-Numb (1:200; Santa Cruz Biotechnology, sc-
294 23579), mouse anti-PH3 (1:2,000; Millipore, 05-806), mouse anti-γTub (1:200; Sigma-
295 Aldrich, T5326) and mouse anti-CD2 (1:50; BioRad). Secondary antibodies conjugated
296 to fluorescent dyes (Invitrogen) were used at 1:400 dilution. Samples were mounted in
297 VECTASHIELD antifade mounting medium for fluorescence (Vector Laboratories, H-
298 1000). Fluorescent images were captured using a Super-resolution Inverted Confocal

299 Microscope Zeiss LSM 880-Airyscan Elyra PS.1. Images were analyzed using the image
300 processing package FIJI from ImageJ and assembled using Adobe Photoshop CS6.
301
302 **GBM microarray**

303 The cohort of patients consisted of seven GBM biopsies obtained from the Valencian
304 Network of Biobanks. The procedures for obtaining tissue samples were developed in
305 accordance with national ethical and legal standards, and following the guidelines
306 established in the Declaration of Helsinki, and approved of Clinical Research Ethics
307 Committee of the Hospital General Universitario de Elche, Spain. All patients had been
308 diagnosed with GBM grade IV, and all of them exhibited an *IDH1* plus *IDH2* wild-type
309 genotype. Normal human brain RNA (frontal lobe; pool from 5 donors) was purchased
310 from BioChain and used as a control for gene expression experiments. A total of
311 12,516 genes were used to generate a custom Agilent Two-Color 8 x 15 K Agilent gene
312 expression DNA microarray, which were deposited in the NCBI Gene Expression
313 Omnibus (GEO) Database under accession number GSE182697 (28).

314 **Bioinformatics analysis**

315 The level of expression of human homologs of *Drosophila* ACD regulators was assessed
316 in seven different GBM patients versus control samples of the custom-made
317 microarray (GSE182697) (28). Statistical analysis of microarray data was done in
318 Multiexperiment Viewer (MeV) (58). Hierarchical clustering analyses were done
319 optimizing gene and sample leaf order and using Pearson Correlation for the distance
320 metric selection. Average linkage clustering was used as a linkage method. For the

321 Gene Distance Matrix (GDM), the distance, inverse of similarity, between two genes
322 was calculated using a distance metric as indicated in MeV.

323 **Human samples and cell lines**

324 Glioma samples were obtained with patients' written informed consent, in accordance
325 with the Declaration of Helsinki, and approved by the Ethics Committee at Hospital 12
326 de Octubre, Madrid, Spain (CEI 14/023). The primary glioblastoma cell lines were
327 provided by the Biobank at "Hospital 12 de Octubre". Fresh tissue samples were
328 enzymatically dissociated using Accumax (Millipore) and cultured in stem cell medium
329 (Neurobasal, Invitrogen), supplemented with N2 (1:100, Invitrogen), GlutaMAX (1:100,
330 Invitrogen), penicillin-streptomycin (1:100, Lonza), 0.4% heparin (Sigma-Aldrich), 40
331 ng/ml EGF and 20 ng/ml bFGF2 (Peprotech). The GB cell lines used in this study were:
332 GB4, GB5, GB7, GB18, GB19, 12o89, Astros (59,60) and HEK293T. The cell lines
333 HEK293T and Astros were maintained in Dulbecco´s modified Eagle Medium
334 supplemented with 10% fetal bovine serum 2 mM L-glutamine, 0.1% penicillin (100
335 U/ml) and streptomycin (100 µg/ml) and Non-Essential Aminoacids (NEA 1x).
336

337 <u>GBM-derived neurosphere cell cultures</u>

338 For stem cell culture of GBM-derived neuroespheres we used DMEM:F12 with FGF-2
339 (20 ng/ml), EGF-2 (20 ng/ml), and N2 supplements, 0.1% penicillin (100 U/ml) and
340 streptomycin (100 µg/ml), as previously described (61,62). The tumor spheres were
341 dissociated to single cells using Accumax, and $1x10^5$ dissociated cells/ml were plated in
342 a Flask and cultured for 6-7 days.
343

344 **In Silico Analysis**

345 Data from The Cancer Genome Atlas (TCGA) and the Chinese Glioma Genome Atlas
346 (CGGA) for GBM cohorts were accessed through UCSC Xena-Browser
347 (https://xenabrowser.net), and Gliovis (http://gliovis.bioinfo.cnio.es) for extraction of
348 overall survival data, gene expression levels, and distribution of genetic alterations.
349 Kaplan-Meier survival curves were generated by stratifying samples into low- and high-
350 expression groups for each gene. Survival differences between these groups were
351 assessed using the log-rank test.

352

353 **DNA Constructs and Lentiviral Production**

354 Lentiviral vectors were used to produce cells overexpressing *RAP2A* (*pLJM1RAP2A*
355 #Plasmid 19311, Addgene) or eGFP (pLJMEGFP #Plasmid 19319, Addgene) as infection
356 control. Infected cells were selected with Puromycin. To obtain the lentivirus, HEK293T
357 cells were transiently co-transfected with 5 µg of the appropriate lentiviral plasmid
358 (pLJEGFP or pLJRRap2A, respectively), 5 µg of the packaging plasmid pCMVdR8.74
359 (#Plasmid 22036, Addgene), and 5 µg of VERSUSV-G envelope protein plasmid pMD2G
360 (#Plasmid 12259, Addgene), using Lipofectamine Plus reagent (Invitrogen, Carisbad,
361 CA, USA). Lentiviral supernatants were collected after 48 h of HEK293T transfection.

362

363 **Neurosphere Immunofluorescences and Imaging**

364 For immunostaining, floating cultured neurospheres were incubated on Matrigel
365 coated micro slide glass for 2 hours at 37°C. After having been washed, the attached
366 neurospheres were fixed in 4% paraformaldehyde for 20 min. Cells were blocked for 1
367 h in 1% FBS and 0.1% Triton X-100 in PBS; then, they were incubated for 2 hours with

368 the primary antibody: mouse anti-CD133 (HB#7, Developmental Studies Hybridoma
369 Bank), mouse anti-Ki67 (3E6, Developmental Studies Hybridoma Bank), rabbit anti-
370 Sox2 (N1C3, GTX101507 GeneTex), mouse anti-Nestin (10c2, sc-23927, Santa Cruz
371 Biotechnology) and mouse anti-Numb (48, sc-136554, Santa Cruz Biotechnology). The
372 secondary antibodies used were Alexa555 goat anti-rabbit (A32732, Invitrogen) or
373 Alexa555 goat anti-mouse (A32727, Invitrogen). Phalloidin 633 (Sigma-Aldrich, 68825
374 Phalloidin-Atto 633) was added and incubated for 20 min in PBS; Vectashield Mounting
375 medium with DAPI (Linaris, H-1200) was added before mounting. Fluorescent images
376 were captured using a Super-resolution Inverted Confocal Microscope Zeiss LSM 880-
377 Airyscan Elyra PS.1. Images were analyzed using the image processing package FIJI
378 from ImageJ and assembled using Adobe Photoshop CS6 program.
379
380 Immunofluorescent quantification
381 Fluorescence intensity measurements were carried out using ImageJ software
382 package. In all cases, images of neuroespheres transfected with GFP (GB5, control) or
383 RAP2A (GB5-RAP2A) lentivirus were analyzed:
384 CD133: Using the "line tool", a line was drawn on the channel with the CD133 signal on
385 three different pictures per genotype. Fluorescence was measured across the line
386 sections with the "Plot Profile Tool", and reported as a subset of images showing the
387 signal intensity plot. For quantification, only the 100 highest gray value points, were
388 taken.
389 Sox: After adjusting the threshold on the channel with the Sox2 signal and eliminating
390 particles smaller than 5 microns, the fluorescence intensity was measured as the mean
391 gray value (sum of all pixels with gray values inside the selection, divided by the

392 number of pixels). In Figure 3 is shown one example out of three quantifications
393 achieved with at least 20 cells per genotype.
394 Nestin: The regions of interest (ROIs) were set with the "hand drawing tool" using the
395 Phalloidin staining to follow the cell periphery. At least 20 cells (ROIs) from three
396 different pictures were selected per condition. The background fluorescence was
397 subtracted from the mean gray value fluorescence for each well, and the fluorescence
398 intensity was normalized by the nuclear DAPI signal coming from the same cell (ROI).
399 Plot in Figure 3C represents the mean gray value that is the sum of all pixels with gray
400 values inside the selection divided by the number of pixels.
401
402 **RNA isolation and qRT-PCR assay**
403 Total RNA was extracted from 7 days old neurospheres using TRI reagent (AM9738,
404 Invitrogen) following manufacturer indications and quantified using a nanodrop (ND-
405 1000, Thermo Scientific). 2ug of RNA was treated with DNaseI (EN0521, Thermo
406 Scientific) and reverse transcribed with SuperScriptTM III Reverse Transcriptase
407 (1808044, Invitrogen). Quantitative real time PCR (qRT-PCR) was performed using
408 Power SYBR Green PCR Master Mix (PN4367218, Applied Biosystems), following
409 established protocols with 60°C for annealing/extension and 40 cycles of amplification
410 on a QuantStudioTM 3 apparatus (applied Biosystems). Act5 primers were used for
411 normalization, and relative expression was calculated using the comparative $\Delta\Delta$Ct. The
412 average of at least 3 independent experiments is shown in Figure 4.
413
414 **Neurosphere Western Blots**

415 Protein extracts were prepared by re-suspending cell pellets in a lysis buffer (50-mM
416 Tris, pH 7.5, 300-mM NaCl, 0.5% SDS, and 1% Triton X-100) and incubating the cells for
417 10 min at 95°C. The lysed extracts were centrifuged at 13,000 g for 10 min at room
418 temperature, and the protein concentration was determined using a commercially
419 available colorimetric assay (BCA Protein Assay Kit). Approximately 25 µg of protein
420 was resolved by 10% or 12,5% SDS-PAGE, and they were then transferred to a PVDF
421 membrane (Hybond-ECL, Amersham Biosciences). The membranes were blocked for
422 1 h at room temperature in TBS-T (10-mM Tris–HCl, pH 7.5, 100-mM NaCl, and 0.1%
423 Tween-20) with 5% skimmed milk, and then incubated overnight at 4°C with the
424 corresponding primary antibody diluted in TBS-T with 2,5% skimmed milk. After
425 washing 3 times with TBS-T, the membranes were incubated for 2 h at room
426 temperature with their corresponding secondary antibody, diluted in TBS-T with 2,5%
427 skimmed milk. The proteins were visible by enhanced chemiluminescence with ECL
428 (Pierce) using Amersham imager 680, and the signal was quantified by Fiji-ImageJ
429 software.
430
431 **Proliferative index (Ki67 analysis)**
432 The number of Ki67+ cells with respect to the total number of nuclei labelled with DAPI
433 within a given neurosphere were counted to calculate the Proliferative Index (PI),
434 which was expressed as the % of Ki67+ cells over total DAPI+ cells. More than 20
435 neurospheres coming from different pictures were analyzed.
436
437 **Sphere size measurement**

438 Glioblastoma cells (GB5 cell line) were infected by control lentivirus (LV-GFP) or by
439 lentivirus directing expression of *RAP2A* (LV-*RAP2A*). The tumor spheres were
440 Accumax-dissociated to single cells, during three consecutive passages. Seven days
441 after the third plating in a 6-well plate, spheres were captured using a 10x objective
442 (Carl Zeiss Axio Imager A1 microscope). 20 random pictures of each genotype were
443 taken and the images were analyzed by measuring the area of all the spheres present,
444 using the "freeform drawing tool" in the ImageJ software package. The data presented
445 show the average area measured in 3 independent experiments.
446
447 **Pair assay and Numb segregation analysis**
448 Dissociated cells were plated at low density (50.000 cells/ml) on Matrigel-coated well
449 glass chamber slides on DMEM: F12 with FGF-2 (20 ng/ml), EGF-2 (20 ng/ml) and N2
450 supplements, 0.1% penicillin (100 U/ml) and streptomycin (100 µg/ml), supplemented
451 with Puromycin. Cultures were incubated for 24, 48 or 72 hours at 37°C with 5% CO_2.
452 Bright field microscopy images from each time point were taken and then the slides
453 were fixed and immunolabeled for Numb, as well as for DAPI to identify nuclei. First,
454 isolated groups of cells (most probably coming from the same single progenitor) were
455 identified and the number of cells in each cluster was annotated. Groups of 3-5 cells
456 were counted in the slide incubated for 48h and groups of 6-8 cells in that incubated
457 for 72h. We did not include in the analysis "neurospheres" with 2 cells, as these can be
458 the result of a symmetric or an asymmetric cell division. We took into account
459 neurospheres with 3-5-7 cells (as odd number of cells) and 4-6-8 cells (as even number
460 of cells).

461 For the Numb analysis, the localization of Numb was visualized and scored in at least
462 100 DAPI-labeled cell pairs. To avoid any artefact, pairs were only captured in the slide
463 incubated for 24h. Images in Figure 6 were acquired in an Inverted Microscope Leica
464 Thunder Imager.
465
466 **Statistical analysis**
467 The data were first analyzed using the Shapiro-Wilk test to determine whether the
468 sample followed a normal distribution. Parametric T-test or a nonparametric two-
469 tailed Mann Whitney U test for those that did not follow a normal distribution were
470 used to compare statistical differences between two different groups. Mean and
471 standard deviation values were calculated by standard methods. A Chi-square test was
472 used to analyze the data in Figure 2C. To assume statistical significance, *p*-values were
473 determined below 0.05. Sample size (n) and the *p*-value are indicated in the figure or
474 figure legend; * $p < 0.05$, ** $p < 0.01$, *** $p < 0.001$, **** $p < 0.0001$; ns: not significant
475 ($p > 0.05$).
476
477
478 **Acknowledgements:** We thank the Bloomington *Drosophila* Stock Center at the
479 University of Indiana and the Developmental Studies Hybridoma Bank at the University
480 of Iowa for kindly providing fly strains and reagents. R.G. was funded by "Instituto de
481 Salud Carlos III (ISCIII)" through the project "Miguel Servet Contracts" (CP21/00116),
482 PI22/01171 and co-funded by the European Union. M.S. was supported by the Spanish
483 grant from the Instituto de Salud Carlos III (ISCIII) PI22/00824. A.C. was financed by the
484 Spanish grants from the Ministry of Science, Innovation and Universities (PGC2018-

097093-B-100), the Ministry of Science and Innovation (PID2021-123196NB-100), the Generalitat Valenciana Prometeo/2021/052 grant and by FEDER (European Regional Development Fund). The "Instituto de Neurociencias" in Alicante is a "Severo Ochoa Center of Excellence in R&D". Our group belongs to "Conexión Cáncer- CSIC".

Author contributions: M.F. participated in the design of the experiments, conducted most of them and analyzed the data; D.B. completed some experiments; R.G. developed the GB lines and performed the in silico analyses; V.M.B. and M.S. carried out the GB microarray and bioinformatics analysis; A.C. conceived the study and wrote the manuscript.

Conflict of interest: The authors declare no competing interests

509 **Figure legends**

510

511 **Figure 1.**

512 ***RAP2A* is highly downregulated in GBM patients**.

513 (**A, B)** Analysis of GBM patient versus control samples focused on the level of

514 expression of human homologs of *Drosophila* ACD regulators by Hierarchical clustering

515 (**A**) and the Gene Distance Matrix (**B**). Color-coded scale bar indicates fold level of

516 expression. **(C)** Kaplan-Meier survival curves corresponding to patients in the TCGA

517 (IDHwt) and Gravendeel (IDHwt) cohort in GBM datasets. Low *RAP2A* expression levels

518 in human GBM are associated with a poor prognosis.

519

520 **Figure 2**.

521 ***Drosophila RAP2A* homolog *Rap2l* regulates ACD.**

522 **(A)** *Drosophila* NBII lineage; the only NB per lineage expresses the transcription factor

523 Dpn, while mature INPs express both Dpn and Ase; iINP, immature INP; mINP, mature

524 INP; GMC, Ganglion Mother Cell. **(B)** Confocal micrographs showing a control larval

525 brain NBII lineage with one NB (Dpn^+ Ase^-) and an NBII lineage in which *Rap2l* has been

526 downregulated displaying an ectopic NB (eNB). **(C)** *Rap2l* downregulation in NBII

527 lineages by the *wor-Gal4 ase-Gal80* (an NBII-specific driver) causes Cno and Numb

528 localization failures (green arrows) in dividing progenitors (NB or INPs), while aPKC

529 localization is not significantly altered (red arrows). Data shown in the scaled bar

530 graphs was analyzed with a U Mann-Whitney test (B) or a Chi-square test (C), $*p<0.05$,

531 $**p<0.01$, ns, not significant, n=number of NB lineages analyzed (in B) or number of

532 dividing cells analyzed (in C); scale bar: 10 μm.

533 **Figure 3.**

534 ***RAP2A* expression in GBM neurosphere cultures reduces the stem cell population.**

535 **(A)** Different GBM cell lines show similar *RAP2A* mRNA levels and significantly lower
536 levels than in control Astros. **(B)** *RAP2A* mRNA levels are significantly higher in the GB5
537 line after infecting this line with *RAP2A* (GB5-RAP2A). Data shown in the scaled bar
538 graphs in A and B was analyzed with an ANOVA and a T-test, respectively; error bars
539 show the SD; n= 2 (in A) and 3 (in B) different experiments. **(C)** Immunofluorescences
540 of the GSC stem cell markers CD133, SOX2 and Nestin reveal a significant reduction in
541 the protein intensity in the GB5 RAP2A-expressing neurospheres (GB5-RAP2A)
542 compared to the control neurospheres (GB5). Data shown in the box plots was
543 analyzed with a U Mann-Whitney for CD133 and Nestin and with a T-test for Sox; the
544 central lines represent the median and the box limits the lower and upper quartiles, as
545 determined by R software; crosses represent sample means; error bars indicate the
546 SEM; n= number of sample points; *p* values: **p*<0.05, ***p*<0.01, ****p*<0.001, ns, not
547 significant; scale bar: 10 μm.

548

549 **Figure 4.**

550 ***RAP2A* expression in GBM neurosphere cultures reduces the stem cell population.**
551 RT-PCRs and Westerns blots show a significant decrease in the mRNA and protein
552 expression levels, respectively, of the GSC markers CD133, SOX2 and Nestin in the GB5
553 RAP2A-expressing neurospheres (GB5-RAP2A) compared to the control neurospheres
554 (GB5). Data shown in the scaled bar graphs was analyzed with an unpaired two-tailed
555 Student´s *t* test; error bars show the SD; n= 3 different experiments; *p* values: **p*<0.05,
556 ***p*<0.01.

557 **Figure 5.**

558 ***RAP2A* expression in GBM neurosphere cultures decreases cell proliferation and**

559 **sphere size.**

560 **(A)** GB5 neurospheres expressing RAP2A (GB5-RAP2A) show a significantly lower

561 number of Ki67 expressing cells per neurosphere than control GB5 neurospheres. Data

562 shown in the box plots was analyzed with a T-test; the central lines represent the

563 median and the box limits the lower and upper quartiles, as determined by R software;

564 crosses represent sample means; error bars indicate the SEM; n= number of sample

565 points. **(B)** GB5 neurospheres expressing RAP2A (GB5-RAP2A) show a significant

566 decrease in their size compared to control GB5 neurospheres of the same stage. Data

567 shown in the scaled bar graphs was analyzed with an unpaired two-tailed Student´s T-

568 test; error bars show the SD; n= total number of neurospheres of 3 different

569 experiments; *p* values: *$p<0.05$; scale bars: 10 μm (in A) and 100μm (in B).

570

571 **Figure 6.**

572 ***RAP2A* expression in GBM neurosphere cultures fosters ACD in GSCs.**

573 **(A)** Early stage GB5 neurospheres expressing RAP2A (GB5-RAP2A) show an odd

574 number of cells (3-5-7) significantly more frequently than control GB5 neurospheres,

575 which show more frequently an even number of cells (4-6-8). **(B)** GB5-RAP2A dividing

576 cells show a significant increase in the number of asymmetric NUMB localization in the

577 progeny, compared to control GB5 dividing cells. Data shown in the bar graphs was

578 analyzed with a Chi-Square test with Yates correction; n= number of neurosphere cell

579 clusters analyzed. *p* values: **$p<0.01$; ***$p<0.001$scale bar: 20 μm.

580

581 **References**

582 1. Knoblich JA. Mechanisms of asymmetric stem cell division. Cell **2008**;132:583-
583 97
584 2. Knoblich JA. Asymmetric cell division: recent developments and their
585 implications for tumour biology. Nat Rev Mol Cell Biol **2010**;11:849-60
586 3. Caussinus E, Gonzalez C. Induction of tumor growth by altered stem-cell
587 asymmetric division in Drosophila melanogaster. Nat Genet **2005**;37:1125-9
588 4. Gateff E. Malignant neoplasms of genetic origin in Drosophila melanogaster.
589 Science **1978**;200:1448-59
590 5. Albertson R, Doe CQ. Dlg, Scrib and Lgl regulate neuroblast cell size and mitotic
591 spindle asymmetry. Nat Cell Biol **2003**;5:166-70
592 6. Bello B, Reichert H, Hirth F. The brain tumor gene negatively regulates neural
593 progenitor cell proliferation in the larval central brain of Drosophila.
594 Development **2006**;133:2639-48
595 7. Betschinger J, Mechtler K, Knoblich JA. Asymmetric segregation of the tumor
596 suppressor brat regulates self-renewal in Drosophila neural stem cells. Cell
597 **2006**;124:1241-53
598 8. Bowman SK, Rolland V, Betschinger J, Kinsey KA, Emery G, Knoblich JA. The
599 tumor suppressors Brat and Numb regulate transit-amplifying neuroblast
600 lineages in Drosophila. Dev Cell **2008**;14:535-46
601 9. Ohshiro T, Yagami T, Zhang C, Matsuzaki F. Role of cortical tumour-suppressor
602 proteins in asymmetric division of Drosophila neuroblast. Nature
603 **2000**;408:593-6
604 10. Peng CY, Manning L, Albertson R, Doe CQ. The tumour-suppressor genes lgl and
605 dlg regulate basal protein targeting in Drosophila neuroblasts. Nature
606 **2000**;408:596-600
607 11. Lee CY, Wilkinson BD, Siegrist SE, Wharton RP, Doe CQ. Brat is a Miranda cargo
608 protein that promotes neuronal differentiation and inhibits neuroblast self-
609 renewal. Dev Cell **2006**;10:441-9
610 12. Bonnet D, Dick JE. Human acute myeloid leukemia is organized as a hierarchy
611 that originates from a primitive hematopoietic cell. Nat Med **1997**;3:730-7
612 13. Lapidot T, Sirard C, Vormoor J, Murdoch B, Hoang T, Caceres-Cortes J*, et al.* A
613 cell initiating human acute myeloid leukaemia after transplantation into SCID
614 mice. Nature **1994**;367:645-8
615 14. Bajaj J, Diaz E, Reya T. Stem cells in cancer initiation and progression. J Cell Biol
616 **2020**;219
617 15. Reya T, Morrison SJ, Clarke MF, Weissman IL. Stem cells, cancer, and cancer
618 stem cells. Nature **2001**;414:105-11
619 16. Moore N, Lyle S. Quiescent, slow-cycling stem cell populations in cancer: a
620 review of the evidence and discussion of significance. J Oncol **2011**;2011
621 17. Rosen JM, Jordan CT. The increasing complexity of the cancer stem cell
622 paradigm. Science **2009**;324:1670-3
623 18. Yadav UP, Singh T, Kumar P, Sharma P, Kaur H, Sharma S*, et al.* Metabolic
624 Adaptations in Cancer Stem Cells. Front Oncol **2020**;10:1010
625 19. Bajaj J, Zimdahl B, Reya T. Fearful symmetry: subversion of asymmetric division
626 in cancer development and progression. Cancer Res **2015**;75:792-7

627 20. Chao S, Yan H, Bu P. Asymmetric division of stem cells and its cancer relevance.
628 Cell Regen **2024**;13:5
629 21. Galli R, Binda E, Orfanelli U, Cipelletti B, Gritti A, De Vitis S*, et al.* Isolation and
630 characterization of tumorigenic, stem-like neural precursors from human
631 glioblastoma. Cancer Res **2004**;64:7011-21
632 22. Singh SK, Clarke ID, Terasaki M, Bonn VE, Hawkins C, Squire J*, et al.*
633 Identification of a cancer stem cell in human brain tumors. Cancer Res
634 **2003**;63:5821-8
635 23. Singh SK, Hawkins C, Clarke ID, Squire JA, Bayani J, Hide T*, et al.* Identification of
636 human brain tumour initiating cells. Nature **2004**;432:396-401
637 24. Biserova K, Jakovlevs A, Uljanovs R, Strumfa I. Cancer Stem Cells: Significance in
638 Origin, Pathogenesis and Treatment of Glioblastoma. Cells **2021**;10
639 25. Chen J, Li Y, Yu TS, McKay RM, Burns DK, Kernie SG*, et al.* A restricted cell
640 population propagates glioblastoma growth after chemotherapy. Nature
641 **2012**;488:522-6
642 26. Hassn Mesrati M, Behrooz AB, Y Abuhamad A, Syahir A. Understanding
643 Glioblastoma Biomarkers: Knocking a Mountain with a Hammer. Cells **2020**;9
644 27. Tang X, Zuo C, Fang P, Liu G, Qiu Y, Huang Y*, et al.* Targeting Glioblastoma Stem
645 Cells: A Review on Biomarkers, Signal Pathways and Targeted Therapy. Front
646 Oncol **2021**;11:701291
647 28. Larriba E, de Juan Romero C, García-Martínez A, Quintanar T, Rodríguez-
648 Lescure Á, Soto JL*, et al.* Identification of new targets for glioblastoma therapy
649 based on a DNA expression microarray. Comput Biol Med **2024**;179:108833
650 29. Chen G, Kong J, Tucker-Burden C, Anand M, Rong Y, Rahman F*, et al.* Human
651 Brat ortholog TRIM3 is a tumor suppressor that regulates asymmetric cell
652 division in glioblastoma. Cancer Res **2014**;74:4536-48
653 30. Wang L, Zhan W, Xie S, Hu J, Shi Q, Zhou X*, et al.* Over-expression of Rap2a
654 inhibits glioma migration and invasion by down-regulating p-AKT. Cell Biol Int
655 **2014**;38:326-34
656 31. Wang L, Zhu B, Wang S, Wu Y, Zhan W, Xie S*, et al.* Regulation of glioma
657 migration and invasion via modification of Rap2a activity by the ubiquitin ligase
658 Nedd4-1. Oncol Rep **2017**;37:2565-74
659 32. Carmena A, Makarova A, Speicher S. The Rap1-Rgl-Ral signaling network
660 regulates neuroblast cortical polarity and spindle orientation. J Cell Biol
661 **2011**;195:553-62
662 33. Bello BC, Izergina N, Caussinus E, Reichert H. Amplification of neural stem cell
663 proliferation by intermediate progenitor cells in Drosophila brain development.
664 Neural Dev **2008**;3:5
665 34. Boone JQ, Doe CQ. Identification of Drosophila type II neuroblast lineages
666 containing transit amplifying ganglion mother cells. Dev Neurobiol
667 **2008**;68:1185-95
668 35. Wodarz A, Ramrath A, Grimm A, Knust E. Drosophila atypical protein kinase C
669 associates with Bazooka and controls polarity of epithelia and neuroblasts. J
670 Cell Biol **2000**;150:1361-74
671 36. Knoblich JA, Jan LY, Jan YN. Asymmetric segregation of Numb and Prospero
672 during cell division. Nature **1995**;377:624-7

673 37. Speicher S, Fischer A, Knoblich J, Carmena A. The PDZ protein Canoe regulates
674 the asymmetric division of Drosophila neuroblasts and muscle progenitors. Curr
675 Biol **2008**;18:831-7
676 38. Gerdes J, Schwab U, Lemke H, Stein H. Production of a mouse monoclonal
677 antibody reactive with a human nuclear antigen associated with cell
678 proliferation. Int J Cancer **1983**;31:13-20
679 39. Sun X, Kaufman PD. Ki-67: more than a proliferation marker. Chromosoma
680 **2018**;127:175-86
681 40. Yan B. Numb--from flies to humans. Brain Dev **2010**;32:293-8
682 41. Morrison SJ, Kimble J. Asymmetric and symmetric stem-cell divisions in
683 development and cancer. Nature **2006**;441:1068-74
684 42. Cayouette M, Raff M. Asymmetric segregation of Numb: a mechanism for
685 neural specification from Drosophila to mammals. Nat Neurosci **2002**;5:1265-9
686 43. Cicalese A, Bonizzi G, Pasi CE, Faretta M, Ronzoni S, Giulini B*, et al.* The tumor
687 suppressor p53 regulates polarity of self-renewing divisions in mammary stem
688 cells. Cell **2009**;138:1083-95
689 44. Ortega-Campos SM, García-Heredia JM. The Multitasker Protein: A Look at the
690 Multiple Capabilities of NUMB. Cells **2023**;12
691 45. Li Z, Zhang YY, Zhang H, Yang J, Chen Y, Lu H. Asymmetric Cell Division and
692 Tumor Heterogeneity. Front Cell Dev Biol **2022**;10:938685
693 46. Dey-Guha I, Wolfer A, Yeh AC, G Albeck J, Darp R, Leon E*, et al.* Asymmetric
694 cancer cell division regulated by AKT. Proc Natl Acad Sci U S A **2011**;108:12845-
695 50
696 47. Sugiarto S, Persson AI, Munoz EG, Waldhuber M, Lamagna C, Andor N*, et al.*
697 Asymmetry-defective oligodendrocyte progenitors are glioma precursors.
698 Cancer Cell **2011**;20:328-40
699 48. Daynac M, Chouchane M, Collins HY, Murphy NE, Andor N, Niu J*, et al.* Lgl1
700 controls NG2 endocytic pathway to regulate oligodendrocyte differentiation
701 and asymmetric cell division and gliomagenesis. Nat Commun **2018**;9:2862
702 49. Bu P, Chen KY, Chen JH, Wang L, Walters J, Shin YJ*, et al.* A microRNA miR-34a-
703 regulated bimodal switch targets Notch in colon cancer stem cells. Cell Stem
704 Cell **2013**;12:602-15
705 50. Hwang WL, Jiang JK, Yang SH, Huang TS, Lan HY, Teng HW*, et al.* MicroRNA-
706 146a directs the symmetric division of Snail-dominant colorectal cancer stem
707 cells. Nat Cell Biol **2014**;16:268-80
708 51. Homem CC, Knoblich JA. Drosophila neuroblasts: a model for stem cell biology.
709 Development **2012**;139:4297-310
710 52. Samanta P, Bhowmik A, Biswas S, Sarkar R, Ghosh R, Pakhira S*, et al.*
711 Therapeutic Effectiveness of Anticancer Agents Targeting Different Signaling
712 Molecules Involved in Asymmetric Division of Cancer Stem Cell. Stem Cell Rev
713 Rep **2023**;19:1283-306
714 53. Chao S, Zhang F, Yan H, Wang L, Zhang L, Wang Z*, et al.* Targeting intratumor
715 heterogeneity suppresses colorectal cancer chemoresistance and metastasis.
716 EMBO Rep **2023**;24:e56416
717 54. Hitomi M, Chumakova AP, Silver DJ, Knudsen AM, Pontius WD, Murphy S*, et al.*
718 Asymmetric cell division promotes therapeutic resistance in glioblastoma stem
719 cells. JCI Insight **2021**;6

720 55. de Thé H. Differentiation therapy revisited. Nat Rev Cancer **2018**;18:117-27
721 56. Neumuller RA, Richter C, Fischer A, Novatchkova M, Neumuller KG, Knoblich JA.
722 Genome-wide analysis of self-renewal in Drosophila neural stem cells by
723 transgenic RNAi. Cell Stem Cell **2011**;8:580-93
724 57. Rives-Quinto N, Franco M, de Torres-Jurado A, Carmena A. Synergism between
725 canoe and scribble mutations causes tumor-like overgrowth via Ras activation
726 in neural stem cells and epithelia. Development **2017**;144:2570-83
727 58. Saeed AI, Sharov V, White J, Li J, Liang W, Bhagabati N*, et al.* TM4: a free, open-
728 source system for microarray data management and analysis. Biotechniques
729 **2003**;34:374-8
730 59. Gargini R, Escoll M, García E, García-Escudero R, Wandosell F, Antón IM. WIP
731 Drives Tumor Progression through YAP/TAZ-Dependent Autonomous Cell
732 Growth. Cell Rep **2016**;17:1962-77
733 60. Gargini R, Segura-Collar B, Herránz B, García-Escudero V, Romero-Bravo A,
734 Núñez FJ*, et al.* The IDH-TAU-EGFR triad defines the neovascular landscape of
735 diffuse gliomas. Sci Transl Med **2020**;12
736 61. Ponti D, Costa A, Zaffaroni N, Pratesi G, Petrangolini G, Coradini D*, et al.*
737 Isolation and in vitro propagation of tumorigenic breast cancer cells with
738 stem/progenitor cell properties. Cancer Res **2005**;65:5506-11
739 62. Gargini R, Cerliani JP, Escoll M, Antón IM, Wandosell F. Cancer stem cell-like
740 phenotype and survival are coordinately regulated by Akt/FoxO/Bim pathway.
741 Stem Cells **2015**;33:646-60
742
743
744
745
746
747
748
749
750
751
752
753
754

755 **Fig S1**. **Statistical analysis of asymmetric cell division expression levels in GBM**
756 **patient samples**. A hierarchical clustering of genes showing significant or non-
757 significant changes in their expression levels is shown. A t-test was applied to the
758 microarray values of the asymmetric cell division regulator genes shown in Fig.1. The
759 statistical values were presented in separate tables corresponding to the significant (**A**)
760 and non-significant (**B**) changes in the indicated genes. The overall threshold *p*-value
761 was 0.01. *p*-values were based on t distribution. Significance was determined using just
762 Alpha.
763
764 **Figure S2. (A)** RAP2A expression levels analysis according to IDHwt GBM subtypes in
765 the TCGA cohort. **(B-D)** Kaplan-Meier survival curves for each GBM subtype, Proneural
766 **(B)**, Mesenchymal **(C)**, and Classical **(D)**, based on high and low RAP2A expression
767 levels.
768
769 **Figure S3. *Drosophila RAP2A* homolog *Rap2l* regulates ACD.** Confocal micrographs
770 showing a control larval brain NBII lineage with one NB (Dpn^+ Ase^-) and NBII lineages in
771 which *Rap2l* has been downregulated displaying an ectopic NB (eNB). The phenotype
772 of three different, independent $Rap2l^{RNAi}$ lines (KK, GD and BDSC) are shown. Data
773 represented in the bar graph was analyzed with a U Mann-Whitney test;
774 ****$p<0.0001$; n=number of NB lineages analyzed; the number of different brains
775 analyzed per genotype is also indicated in brackets.

Figure 1

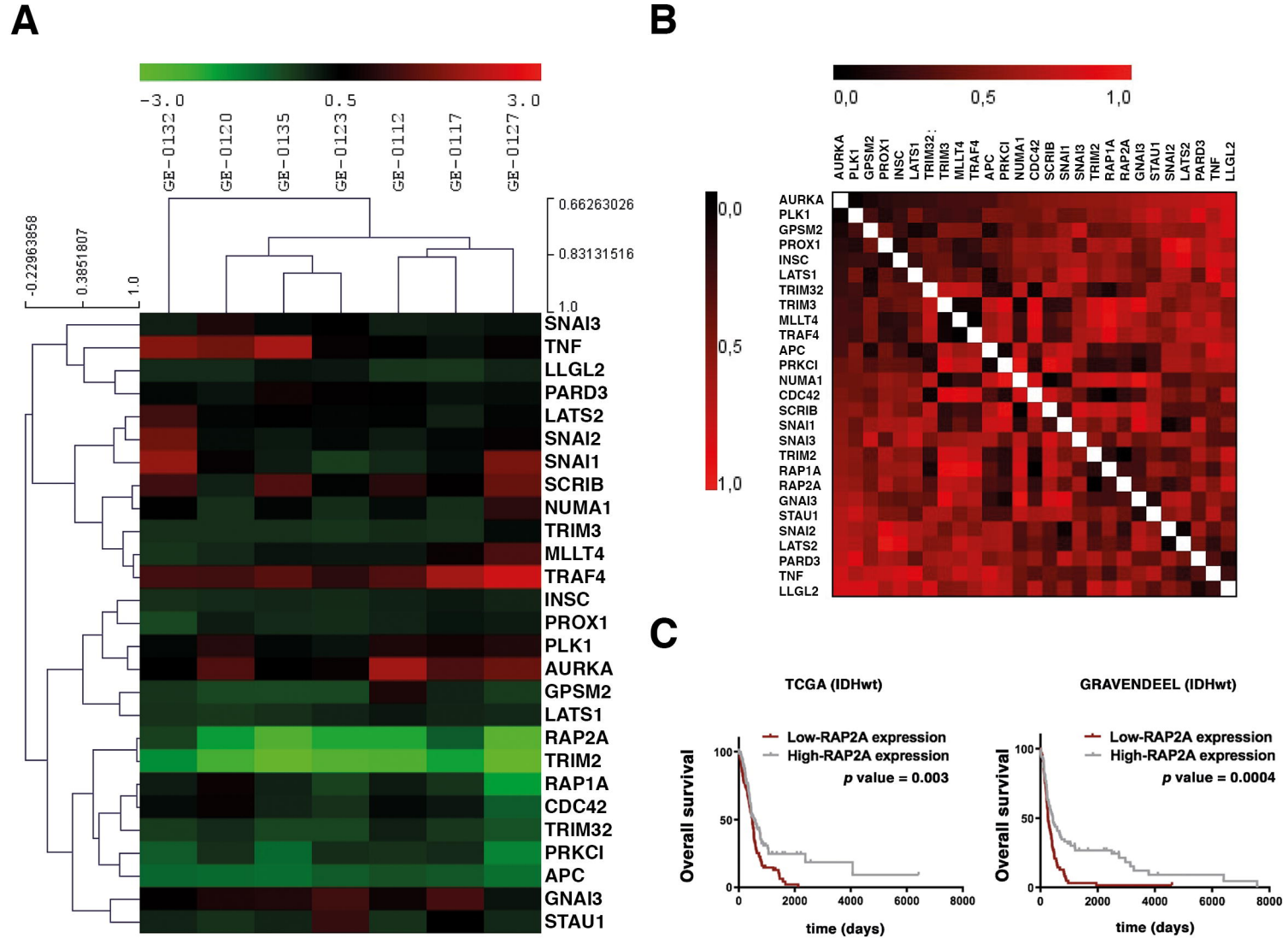
A
-3.0
0.5
3.0
GE-0132
GE-0120
GE-0135
GE-0123
GE-0112
GE-0117
GE-0127
-0.22963858
0.3851807
1.0
0.66263026
0.83131516
1.0
SNAI3
TNF
LLGL2
PARD3
LATS2
SNAI2
SNAI1
SCRIB
NUMA1
TRIM3
MLLT4
TRAF4
INSC
PROX1
PLK1
AURKA
GPSM2
LATS1
RAP2A
TRIM2
RAP1A
CDC42
TRIM32
PRKCI
APC
GNAI3
STAU1
B
0,0
0,5
1,0
AURKA
PLK1
GPSM2
PROX1
INSC
LATS1
TRIM32
TRIM3
MLLT4
TRAF4
APC
PRKCI
NUMA1
CDC42
SCRIB
SNAI1
SNAI3
TRIM2
RAP1A
RAP2A
GNAI3
STAU1
SNAI2
LATS2
PARD3
TNF
LLGL2
C
TCGA (IDHwt)
Low-RAP2A expression
High-RAP2A expression
p value = 0.003
Overall survival
time (days)
GRAVENDEEL (IDHwt)
Low-RAP2A expression
High-RAP2A expression
p value = 0.0004
Overall survival
time (days)

Figure 2

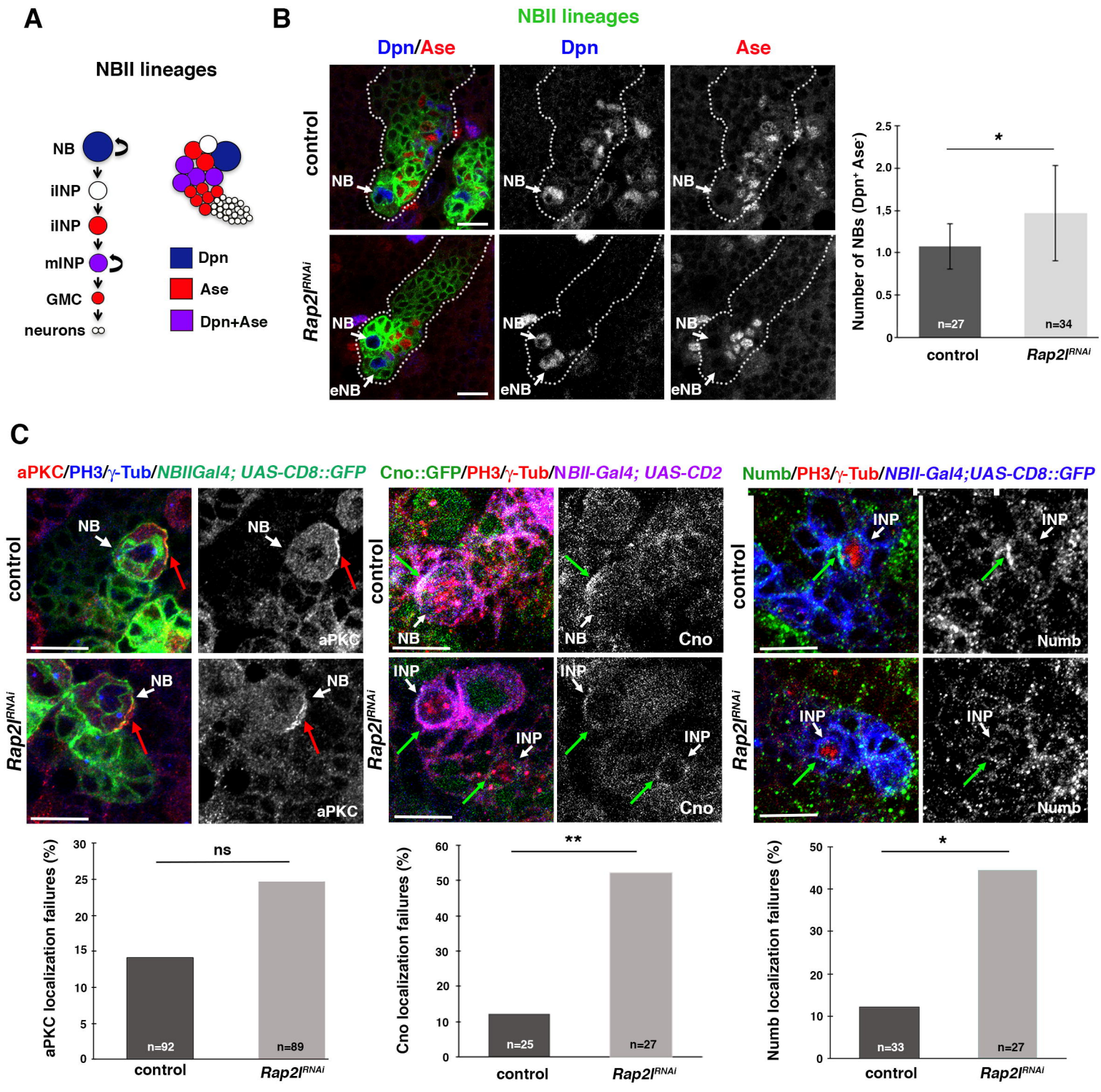
A
NBII lineages
NB
iINP
iINP
mINP
GMC
neurons
Dpn
Ase
Dpn+Ase
B
NBII lineages
Dpn/Ase
Dpn
Ase
control
Rap2l RNAi
NB
eNB
Number of NBs (Dpn+ Ase-)
n=27
n=34
control
Rap2l RNAi
C
aPKC/PH3/γ-Tub/NBIIGal4; UAS-CD8::GFP
Cno::GFP/PH3/γ-Tub/NBII-Gal4; UAS-CD2
Numb/PH3/γ-Tub/NBII-Gal4;UAS-CD8::GFP
INP
aPKC
Cno
Numb
aPKC localization failures (%)
ns
n=92
n=89
Cno localization failures (%)
**
n=25
n=27
Numb localization failures (%)
*
n=33
n=27

Figure 3

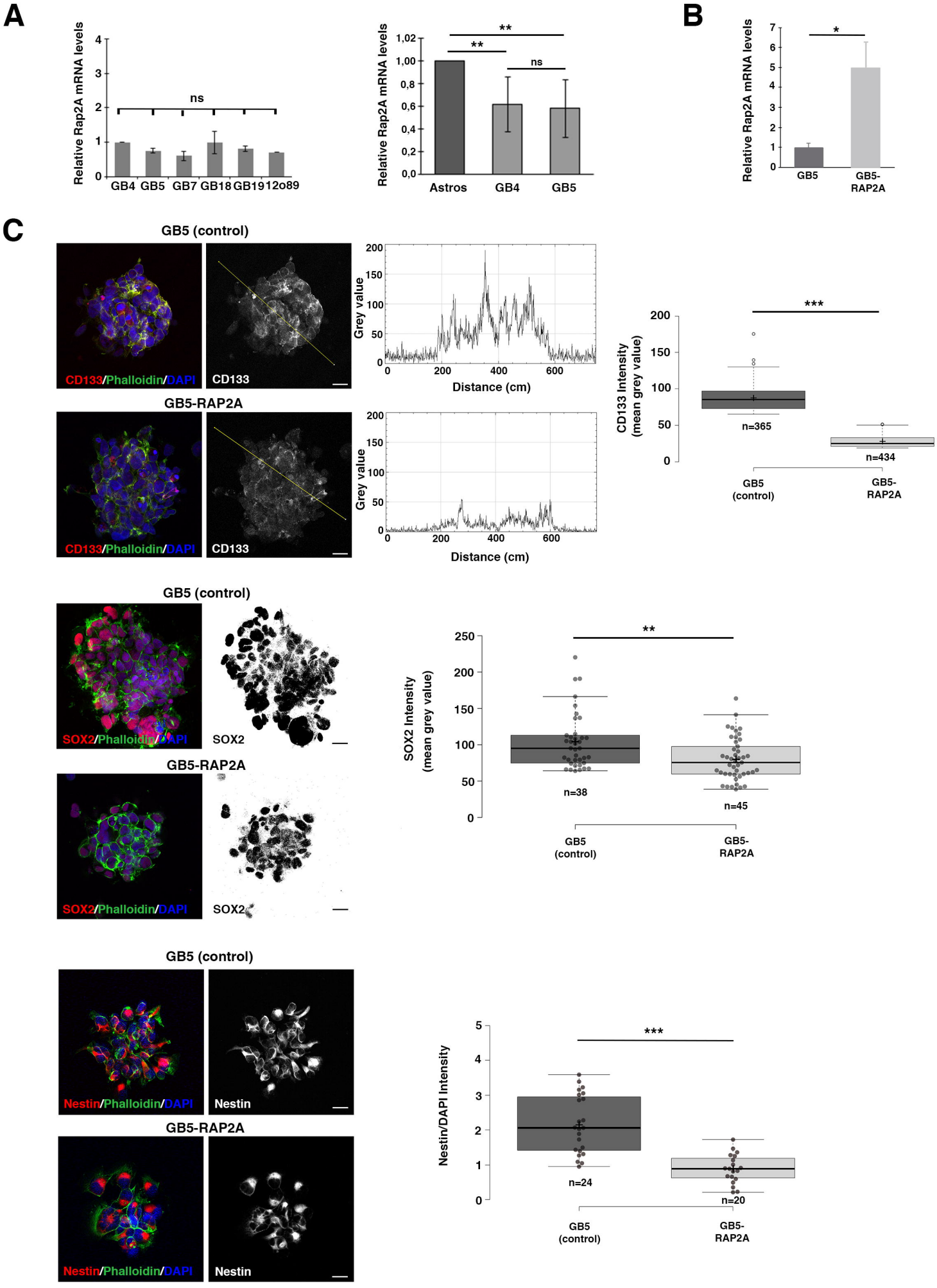
A
Relative Rap2A mRNA levels
ns
GB4 GB5 GB7 GB18 GB19 12o89
Relative Rap2A mRNA levels
**
**
ns
Astros GB4 GB5
B
Relative Rap2A mRNA levels
*
GB5 GB5-RAP2A
C
GB5 (control)
CD133/Phalloidin/DAPI
CD133
Grey value
Distance (cm)
GB5-RAP2A
CD133 Intensity (mean grey value)
***
n=365
n=434
GB5 (control) GB5-RAP2A
SOX2/Phalloidin/DAPI
SOX2
SOX2 Intensity (mean grey value)
**
n=38
n=45
Nestin/Phalloidin/DAPI
Nestin
Nestin/DAPI Intensity
***
n=24
n=20

Figure 4

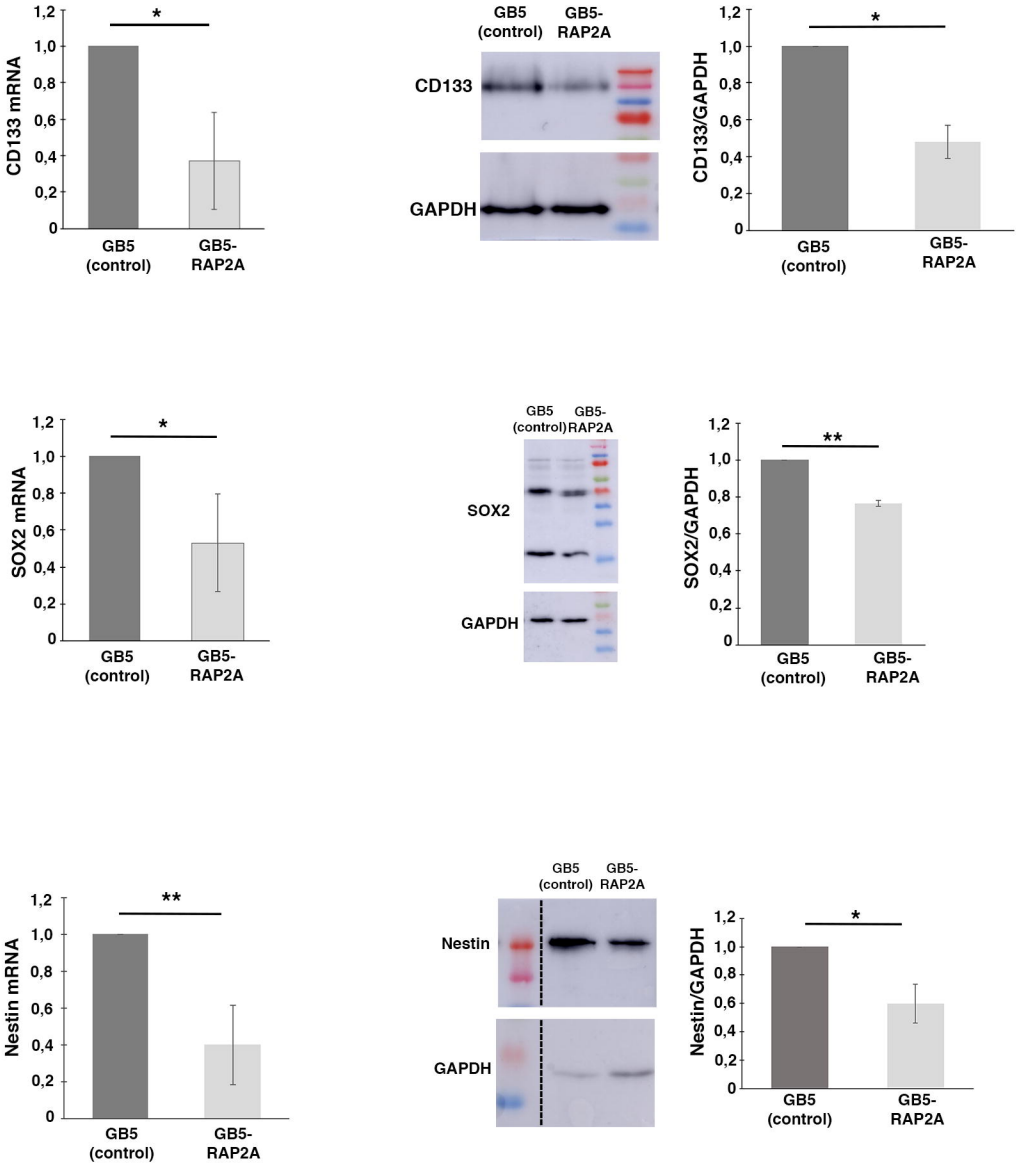
CD133 mRNA
1,2
1,0
0,8
0,6
0,4
0,2
0
*
GB5 (control)
GB5-RAP2A
GB5 (control)
GB5-RAP2A
CD133
GAPDH
CD133/GAPDH
*
SOX2 mRNA
*
SOX2
GAPDH
SOX2/GAPDH
**
Nestin mRNA
**
Nestin
GAPDH
Nestin/GAPDH
*

Figure 5

A

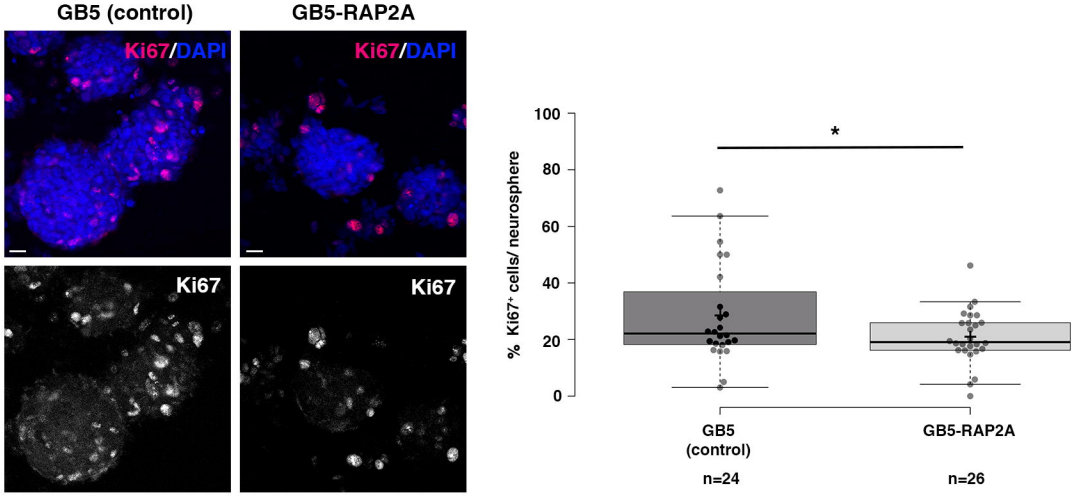
GB5 (control)
GB5-RAP2A
Ki67/DAPI
Ki67/DAPI
Ki67
Ki67
% Ki67+ cells/ neurosphere
100
80
60
40
20
0
*
GB5
(control)
GB5-RAP2A
n=24
n=26

B

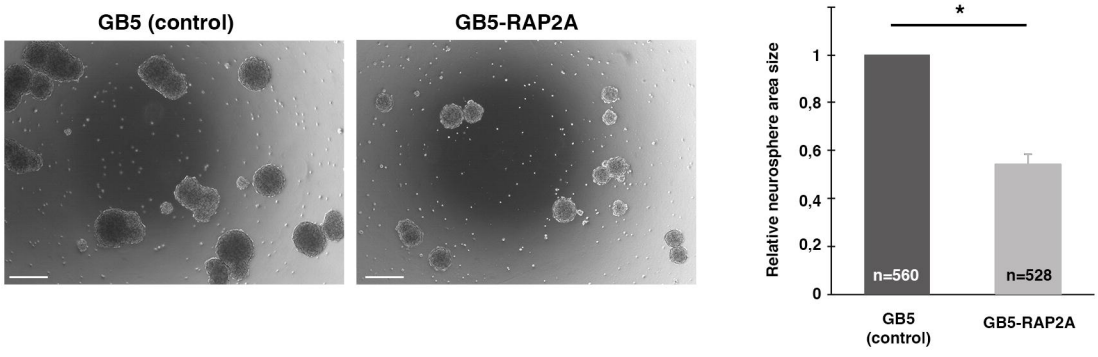
GB5 (control)
GB5-RAP2A
Relative neurosphere area size
1
0,8
0,6
0,4
0,2
0
*
n=560
n=528
GB5
(control)
GB5-RAP2A

Figure 6

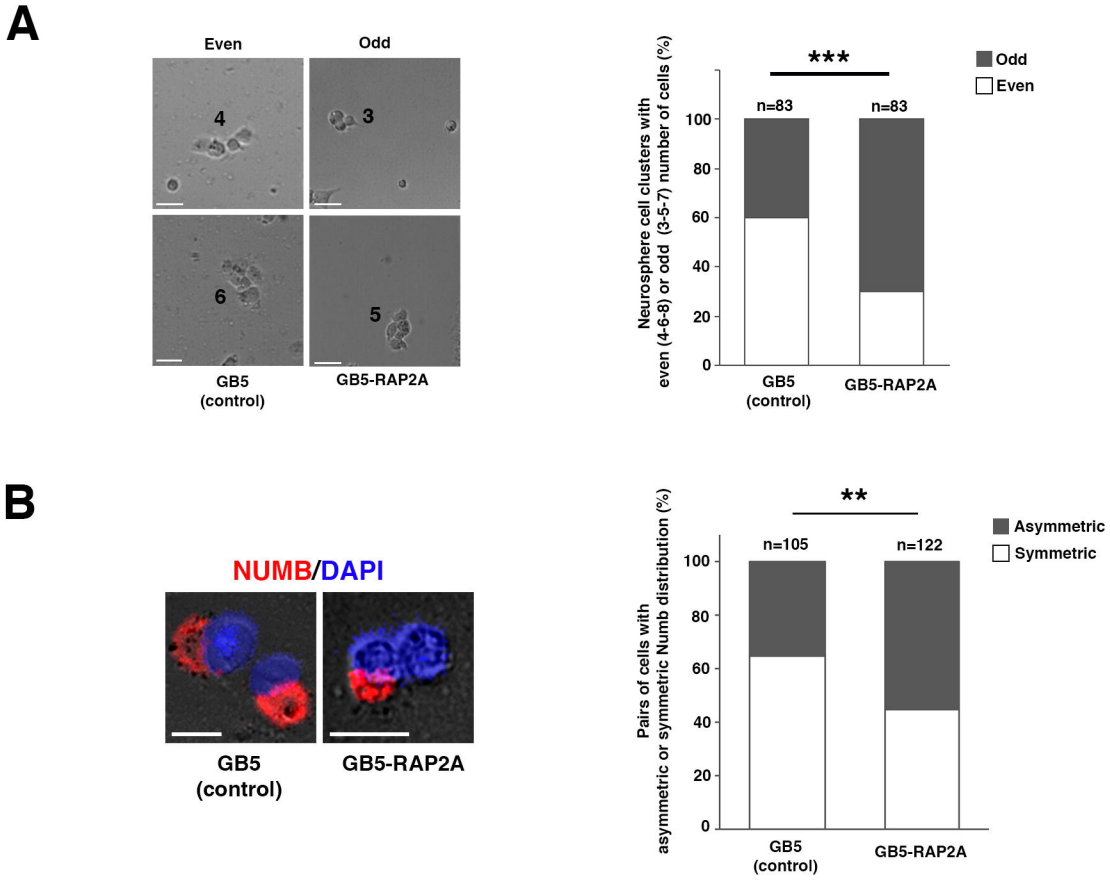
A
Even
Odd
4
3
6
5
GB5
(control)
GB5-RAP2A
***
Odd
Even
n=83
n=83
Neurosphere cell clusters with
even (4-6-8) or odd (3-5-7) number of cells (%)
100
80
60
40
20
0
GB5
(control)
GB5-RAP2A
B
NUMB/DAPI
GB5
(control)
GB5-RAP2A
**
Asymmetric
Symmetric
n=105
n=122
Pairs of cells with
asymmetric or symmetric Numb distribution (%)
100
80
60
40
20
0
GB5
(control)
GB5-RAP2A